Available online at www.sciencedirect.com
ScienceDirect
Ultramicroscopy 108 (2008) 84–99
ultramicroscopy
www.elsevier.com/locate/ultramic

The impact of surface and retardation losses on valence electron energy-loss spectroscopy

Rolf Erni[a,*], Nigel D. Browning[b,c]

[a]EMAT, University of Antwerp, Groenenborgerlaan 171, B 2020 Antwerp, Belgium
[b]Materials Science and Technology Division, Lawrence Livermore National Laboratory, P.O. Box 808, L-356, Livermore, CA 94550, USA
[c]Department of Chemical Engineering and Materials Science, University of California Davis, One Shields Ave., Davis, CA 95616, USA

Received 11 December 2006; received in revised form 8 March 2007; accepted 20 March 2007

Abstract

The inelastic scattering of fast electrons transmitting thin foils of silicon (Si), silicon nitride (Si_3N_4), gallium arsenide (GaAs), gallium nitride (GaN) and cadmium selenide (CdSe) was analyzed using dielectric theory. In particular, the impact of surface and bulk retardation losses on valence electron energy-loss spectroscopy (VEELS) was studied as a function of the foil thickness. It is shown that for the materials analyzed, surface and retardation losses can cause a systematic, thickness-dependent modulation of the dielectric volume losses, which can hamper the determination of the bulk dielectric data as well as the identification of band-gap and interband transition energies by VEELS. For Si and GaAs, where the dielectric function is strongly peaked with high absolute values, retardation losses lead to additional intensity maxima in the spectrum. For thin films of these materials (below ~100 nm), the additional intensity maxima are related to retardation effects due to the finite size of the sample leading to the excitation of guided light modes. For thicker films, exceeding about 200 nm, the intensity maxima are caused by bulk retardation losses, i.e., Cerenkov losses. Although thickness-dependent modulations were observed for Si_3N_4, GaN and CdSe, the form of the dielectric functions and their lower maxima, means that for TEM samples <100 nm thick, the band-gap energies of these materials can be accurately identified by VEELS. Guidelines are given that allow for forecasting the impact of surface and retardation losses on VEELS.

PACS: 68.37.Lp; 79.20.Uv; 78.30.Am

Keywords: S/TEM; VEELS; Semiconductors; Retardation effects; Surface effects; Si; Si_3N_4; GaAs; GaN; CdSe

1. Introduction

For a variety of different materials, valence electron energy-loss spectroscopy (VEELS) carried out in (scanning) transmission electron microscopy has been used for measuring band structure information and in particular for identifying band-gap energies (see, e.g., [1–5]). In most cases band structure information extracted from VEEL spectra coincides with information obtained by other techniques like, e.g., by vacuum ultraviolet spectroscopy or by spectroscopic ellipsometry (see, e.g., [6]). Compared to other methods, the advantage of performing band structure measurements by VEELS in a (scanning) transmission electron microscope is the spatial resolution; band-gap measurements with a spatial resolution down to ~1 nm are feasible [7]. Furthermore, the recent implementation of monochromated (scanning) transmission electron microscopes has made VEELS an easily applicable tool to locally study the band structure of complex semiconductor architectures. The improved energy resolution of monochromated instruments (<200 meV) significantly simplifies the interpretation of VEELS data [8–10]. However, although VEELS has successfully been applied for many years, the relative importance of surface and retardation losses [11–13] over bulk dielectric losses, has not been resolved.

Thin foils of materials, typically below 100 nm in thickness, are used for electron energy-loss spectroscopy in (scanning) transmission electron microscopy (S/TEM). If a charged particles moves from one dielectric medium to

*Corresponding author. Tel.: +32 3 265 3259; fax: +32 3 2653257.
E-mail address: rolf.erni@ua.ac.be (R. Erni).

0304-3991/$ - see front matter © 2007 Elsevier B.V. All rights reserved.
doi:10.1016/j.ultramic.2007.03.005

another, it can excite collective oscillations of surface (or interface) electrons. Surface (or interface) plasmons are longitudinal waves of the surface (or interface) charge density that run along the boundary. For a thin foil transmitted by fast electrons, the excitation of the upper and the lower surface can be coupled. This leads to thickness-dependent excitation modes of surface electrons and to the corresponding energy losses in the transmitted electron beam [14]. Therefore, the impact of surface losses in the pre-plasmon spectral region is not a priori negligible.

Secondly, a fast electron interacting with a solid can be impacted by retardation effects. The retardation of the electron essentially alters the scattering distribution in the (E, θ)-plane, where θ is the scattering angle and E is the energy loss [15,16]. For materials with a high dielectric constant (real part ε_1), retardation of the incident electrons can lead to the emission of Cerenkov radiation and to the corresponding energy losses in the transmitted beam. Generally, Cerenkov radiation can be emitted, if a charged particle moves faster inside a medium than the light inside this medium, i.e., if $v > c/\sqrt{\varepsilon_1(E)}$ is fulfilled. The relativistic speed of the charged particle (the electron) is v, c is the speed of light in vacuum, E is the energy (loss) and $\varepsilon_1(E)$ is the real part of the dielectric function. This condition defines for a given value of ε_1 a critical electron energy eV_c above which Cerenkov losses become feasible. For many semiconductor materials ε_1 is large enough such that Cerenkov radiation can in principle be emitted at acceleration voltages common in (S)TEM. In these cases, the potential impact of Cerenkov losses on dielectric absorption features in VEELS has to be considered. The probability of the emission of Cerenkov radiation increases with increasing ε_1. Hence, Cerenkov losses are typically peaked on the energy-loss axis where the real part of the dielectric function ε_1 is maximal [17]. Cerenkov absorption features thus fall exactly in the spectral region where band structure and band gap information is contained.

The thickness of the thin films commonly used in (S)TEM limits however the emission of Cerenkov radiation and the appearance of Cerenkov losses in VEELS. In the case of very thin foils, the Cerenkov light cone cannot be built up and no Cerenkov radiation can be emitted—even if the bulk condition for the emission of Cerenkov radiation given above is fulfilled [12,17]. As a rule of thumb; if the thickness of the foil is smaller than the wavelength of the Cerenkov radiation, the emission of Cerenkov radiation is inhibited and Cerenkov losses are absent in VEELS. Although the thickness restriction is not strictly formulated here (for a detailed treatment see [12,17]), it shows that the probability of Cerenkov losses for typical TEM foils (<100 nm) is small. Similar to small particles, very thin TEM foils do not show bulk Cerenkov losses in VEELS [12].

Surface, interface and finite-size effects, potentially related to the retardation of the electron, can be important in the case of thin films. Which excitation modes are feasible, depends on the magnitude of the real part ε_1 of the material's dielectric function. If an electron passes through a metal whose dielectric function ε_1 goes through zero, radiative surface plasmons can be excited. Energy losses caused by the excitation of a radiative surface plasmon are superimposed on the volume plasmon loss, show however a different θ dependency. The energy losses related to the radiative surface plasmons are equal or larger than the energy losses caused by the excitation of the volume plasmon [18]. Radiative surface plasmons decay by emitting light. Non-radiative surface plasmons can be excited by transmitting electrons, if the material's dielectric function ε_1 becomes smaller than -1. The corresponding energy losses show a characteristic dispersion; the energy losses are smaller than the losses related to the actual surface plasmon mode $E_S(\theta)$, approaching however E_S for large θ [14]. If the real part ε_1 of the material's dielectric function becomes larger than 1, retardation effects can occur. If the primary electron energy is large enough, electrons can then excite radiative or non-radiative guided light modes [19]. In the present case where the low-loss scattering of materials of high dielectric constants is analyzed (silicon (Si), silicon nitride (Si_3N_4), gallium arsenide (GaAs), gallium nitride (GaN) and cadmium selenide (CdSe)), non-radiative guided light modes have to be considered. A surface (or interface) plasmon corresponds to an excitation mode of the surface charge density, leading to a longitudinal electromagnetic wave that propagates with a given phase velocity parallel to the boundary. The maximum amplitude of the electromagnetic wave associated with a surface plasmon is located at the surface. Compared to a surface plasmon, a guided light mode involves collective excitations of electrons inside the foil. The component parallel to the foil normal of the electromagnetic field associated with a guided light mode is a standing wave that shows one (or more) amplitude maximum (maxima) within the foil, whereas at the boundary of the material the amplitude is small. The electromagnetic wave propagates with a given phase velocity parallel to the foil [14]. A surface (or interface) plasmon is determined by the boundary configuration, whereas a guided light mode is essentially determined by the finite thickness (or finite size) of the sample. If the condition for total internal reflection is not fulfilled, a guided light mode can decay by emitting light. Similar to a radiative surface plasmon, a guided light mode is then called radiative.

Guided modes can also be excited through coupling to Cerenkov radiation. If the opening angle of the Cerenkov light cone is larger than the angle of total internal reflection, no Cerenkov radiation can be emitted. In such cases, the retardation radiation is confined within the sample at guided mode frequencies [12].

From the analysis of VEELS data recorded in (S)TEM, band-gap energies, interband transition energies and the dielectric function can be determined. Such analyses are usually done under the assumption that the VEELS data contain solely bulk dielectric data and that potential contributions of surface and retardation losses are negligible (see, e.g., [1,2,5,6,10,20,21]). In the present work, it is assumed that the dielectric function of the material is

known. On the basis of the dielectric theory, VEEL spectra of Si, Si_3N_4, GaAs, GaN and CdSe are calculated as a function of the foil thickness taking into account energy losses that are due to retardation, finite size and surface effects. Knowing the bulk dielectric function and its intrinsic contribution to the low loss scattering, the impact of retardation, finite size and surface effects on VEEL spectra can be revealed. It is shown that although all the materials investigated potentially show retardation effects, careful differentiation is necessary. Practical guidelines are given that allow for estimating the impact of retardation, finite size and surface effects on VEELS data. These guidelines can be used either to forecast the impact of these contributions or to estimate a posteriori their "hidden" impact on dielectric data determined by VEELS.

2. Inelastic electron scattering by thin films

This section summarizes the formalism used to calculate the low-loss inelastic electron scattering probability on the basis of the dielectric theory. More detailed information about this concept can be found in, e.g., Refs. [14,15,17,22]. It is assumed that the electrons penetrate the foils parallel to the foil normal and, that inelastically scattered electrons are detected in forward direction within a given opening angle determined by the spectrometer's collection angle θ_C. For the small scattering angles considered, the θ-dependency of the dielectric function is not taken into account; the dispersion of the volume plasmon and any other bulk dielectric property are neglected.

2.1. Loss probability: non-retarded volume and surface effects

In this sub-section, two expressions are given which describe the inelastic scattering probability of fast electrons interacting with thin films. The first expression gives the loss probability due to the volume of the foil, the second expression takes volume and surface contributions into account. Retardation effects are not considered, i.e., $\beta = v/c$ is set equal zero.

On the basis of the dielectric function of a solid, Ritchie [23] derived a semi-classical expression that describes the inelastic scattering of a fast electron interacting with a thin foil. The probability $P_{\mathrm{vol,nr}}$ that an electron is inelastically scattered by transmitting a thin foil of thickness t can be expressed as [17,23,24]

$$\frac{\partial^2 P_{\mathrm{vol,nr}}}{\partial E \partial \Omega}(E,\theta) = \left(\frac{e^3}{4\pi^3\hbar^2\varepsilon_0 v^2}\right) \mathrm{Im}\left(\frac{1}{\hat{\varepsilon}(E)}\right) \frac{t}{\theta^2+\theta_E^2}. \tag{1}$$

This expression describes the double-differential scattering probability $P_{\mathrm{vol,nr}}$ due to volume interactions in units of 1/(eV srad) where E is the energy loss and Ω the solid angle. In Eq. (1), $\hat{\varepsilon}(E)$ is the complex conjugate of the dielectric function of the material; $\hat{\varepsilon} = \varepsilon_1 - i\varepsilon_2$, where ε_1 and ε_2 are the real and the imaginary part of the complex dielectric function ε, and θ_E is the characteristic scattering angle for an energy loss E. Eq. (1), describing the bulk dielectric losses, is the fundamental relation on which most VEEL spectra have been analyzed (see, e.g., [3,4,10,21,25]).

Including surface contributions, the double-differential scattering probability becomes [17,23]

$$\frac{\partial^2 P_{\mathrm{nr}}}{\partial E \partial \Omega}(E,\theta) = \left(\frac{\mathrm{e}^3}{4\pi^3\hbar^2\varepsilon_0 v^2}\right) \times \mathrm{Im}\left(\frac{t}{\hat{\varepsilon}\varphi^2} - \frac{2\theta^2(\hat{\varepsilon}-\hat{\eta})^2}{\hat{\varepsilon}\hat{\eta}\varphi^4}\frac{\hbar}{m_\mathrm{e} v}\left[\frac{\sin^2 d_\mathrm{e}}{L^+} + \frac{\cos^2 d_\mathrm{e}}{L^-}\right]\right). \tag{2.1}$$

The complex conjugate of the dielectric function of the surrounding medium is $\hat{\eta}(E)$, m_e is the rest mass of the electron and

$$\varphi^2 = \lambda^2 + \theta_E^2, \tag{2.2}$$

$$\lambda^2 = \theta^2 - \hat{\varepsilon}\theta_E^2\beta^2, \tag{2.3}$$

$$\lambda_0^2 = \theta^2 - \hat{\eta}\theta_E^2\beta^2, \tag{2.4}$$

$$d_\mathrm{e} = (tE)/(2\hbar v), \tag{2.5}$$

$$L^+ = \lambda_0\hat{\varepsilon} + \lambda\hat{\eta}\tanh\left(\frac{\lambda d_\mathrm{e}}{\theta_E}\right) \tag{2.6}$$

and

$$L^- = \lambda_0\hat{\varepsilon} + \lambda\hat{\eta}\coth\left(\frac{\lambda d_\mathrm{e}}{\theta_E}\right). \tag{2.7}$$

Eq. (2) describes the probability that an electron is inelastically scattered on transmitting a thin foil including finite size effects and the interaction with the surface of the foil. The conditions $|L^+(\theta,E)| = \mathrm{Min.}$ and $|L^-(\theta,E)| = \mathrm{Min.}$ describe the dispersion relations of the surface excitation. As mentioned above, since retardation effects are not taken into account within this subsection, β is set equal zero. Depending on the choice of the complex dielectric function of the surrounding medium η, either a surface, or an interface can be analyzed. Analogous to ε, η is in general a function of complex value; for the case that the foil is in vacuum $\eta(E) = \eta = 1$.

2.2. Loss probability: volume, surface and retardation effects

Taking retardation effects into account ($\beta \neq 0$), the volume contribution given in Eq. (1) becomes [15,17,24]

$$\frac{\partial^2 P_{\mathrm{vol}}}{\partial E \partial \Omega}(E,\theta) = \left(\frac{\mathrm{e}^3}{4\pi^3\hbar^2\varepsilon_0 v^2}\right) \mathrm{Im}\left(\frac{1}{\hat{\varepsilon}(E)}\right) t \times \frac{\theta^2+\theta_E^2\left[\left(1-\varepsilon_1\beta^2\right)^2 + \left(\varepsilon_2\beta^2\right)^2\right]}{\left[\theta^2+\theta_E^2\left(1-\varepsilon_1\beta^2\right)\right]^2 + \left(\theta_E^2\varepsilon_2\beta^2\right)^2}. \tag{3}$$

Eq. (3) describes the probability that an electron is inelastically scattered on transmitting a thin foil of

thickness t including retardation effects ignoring, however, any interaction with the surface of the foil. For the non-retarded case, i.e., $\beta \to 0$, Eq. (3) becomes equal to Eq. (1). If volume and surface contributions are taken into account, the differential scattering probability becomes [15,17]

$$\frac{\partial^2 P}{\partial E \partial \Omega}(E,\theta) = \left(\frac{e^3}{4\pi^3 \hbar^2 \varepsilon_0 v^2}\right) \mathrm{Im}\left(\frac{t\mu^2}{\hat{\varepsilon}\varphi^2} - \frac{2\theta^2(\hat{\varepsilon}-\hat{\eta})^2}{\varphi_0^4 \varphi^4}\frac{\hbar}{m_e v}\{A+B+C\}\right). \tag{4.1}$$

With the terms A, B and C given by

$$A = \frac{\varphi_{01}^4}{\hat{\varepsilon}\hat{\eta}}\left(\frac{\sin^2 d_e}{L^+} + \frac{\cos^2 d_e}{L^-}\right), \tag{4.2}$$

$$B = \beta^2 \frac{\lambda_0}{\hat{\eta}}\theta_E \varphi_{01}^2 \left(\frac{1}{L^+} - \frac{1}{L^-}\right)\sin(2d_e), \tag{4.3}$$

$$C = -\beta^4 \lambda_0 \lambda \theta_E^2 \left(\frac{\cos^2 d_e \tanh\left(\lambda \frac{d_e}{\theta_E}\right)}{L^+} + \frac{\sin^2 d_e \coth\left(\lambda \frac{d_e}{\theta_E}\right)}{L^-}\right) \tag{4.4}$$

and with

$$\mu^2 = 1 - \hat{\varepsilon}\beta^2, \tag{4.5}$$

$$\varphi_0^2 = \lambda_0^2 + \theta_E^2 \tag{4.6}$$

and

$$\varphi_{01}^2 = \theta^2 + \theta_E^2\left(1 - (\hat{\varepsilon}-\hat{\eta})\beta^2\right). \tag{4.7}$$

The Kröger formula, Eq. (4), describes the (single-scattering) energy-loss function in transmission electron energy-loss spectroscopy for the case that volume, surface and retardation effects are taken into account. In order to calculate VEEL spectra, the double-differential scattering probability is integrated over the detection area

$$\frac{\partial P}{\partial E}(E) = 2\pi \int_0^{\theta_C} \frac{\partial^2 P_i}{\partial E \partial \Omega}(E,\theta)\sin\theta \, \mathrm{d}\theta. \tag{5}$$

Eq. (5) gives the single scattering contribution of VEEL spectra assuming parallel illumination. The probability function P_i on the right side of Eq. (5) is either taken from Eqs. (1)–(3), or (4).

3. Experimental details

Low-loss electron energy-loss spectra were recorded on transmission electron microscopes equipped with a Wien-filter type electron monochromator (see, e.g., Ref. [10] and references therein). The spectra of Si_3N_4, GaN and GaAs were recorded using a monochromated FEI Tecnai F20 microscope operated at 200 kV in diffraction mode using a collection angle of 2.1 mrad and a probe semi-convergence angle of ~20 mrad (National Center for Electron Microscopy, Lawrence Berkeley National Laboratory, California, USA). The Si data were recorded on a monochromated FEI Titan 80–300 equipped with an illumination C_S corrector operated at 300 kV in diffraction mode using a collection angle of 3.8 mrad and a probe semi-convergence angle of 19 mrad (Ernst-Ruska Center, Forschungszentrum Jülich, Germany). The Tecnai microscope operated at 200 kV allowed for an energy resolution of 200 meV, the Titan microscope operated at 300 kV was setup in order to achieve an energy resolution of 160 meV. The contribution of the zero-loss peak was removed by locally fitting a power-law function in front of the first absorption feature. This background correction is adequate for identifying the dominant absorption features, but does not guarantee accurate quantification of the low-loss scattering. Furthermore, low and very smoothly modulated retardation contributions in front of a distinct band-gap signal might not be properly considered with this background removal technique.

The scattering probabilities and VEEL spectra were calculated within the dielectric formalism summarized in Section 2. The (optical) dielectric data of Si, Si_3N_4 and GaAs were taken from Palik [26]. The dielectric data of GaN is based on spectroscopic ellipsometry measured perpendicular to the [0 0 0 1] axis taken from Kawashima et al. [27]. The same geometry was employed to record the experimental VEELS data of GaN. The dielectric data of wurtzite CdSe, parallel to the [0 0 0 1] axis, were taken from [28]. All spectra shown are normalized such that the maximum intensity is equal 1 within the area of interest.

VEEL spectra were calculated for a collection angle of 2.1 mrad. The effective collection angles of the experiments performed are clearly larger. However, for the geometrical setup described in Section 2, the inelastic electron scattering dominating the low-loss signal can be found at small scattering angles, below ~0.1 mrad. This circumstance reasons why the calculations can be compared with experimental data that were recorded using significantly larger (effective) collection angles.

4. Results

4.1. Si

Fig. 1 shows calculated scattering probabilities in the (E,θ)-plane of 300 keV electrons transmitting a 50 nm thick foil of Si. The scattering probability $P_{vol,nr}$ of the non-retarded volume contribution according to Eq. (1) is depicted in Fig. 1(a). Fig. 1(b) shows the volume scattering probability P_{vol} including retardation effects according to Eq. (3) and the scattering probability P considering volume, surface and retardation effects according to Eq. (4) is given in Fig. 1(c). The schematics in Fig. 1(d) identifies some of the absorption features; the broad peak around 16.5 eV is caused by the excitation of the volume plasmon, and the features at $E = 3.4$ and 4.2 eV can be attributed to interband transitions. As the dielectric data

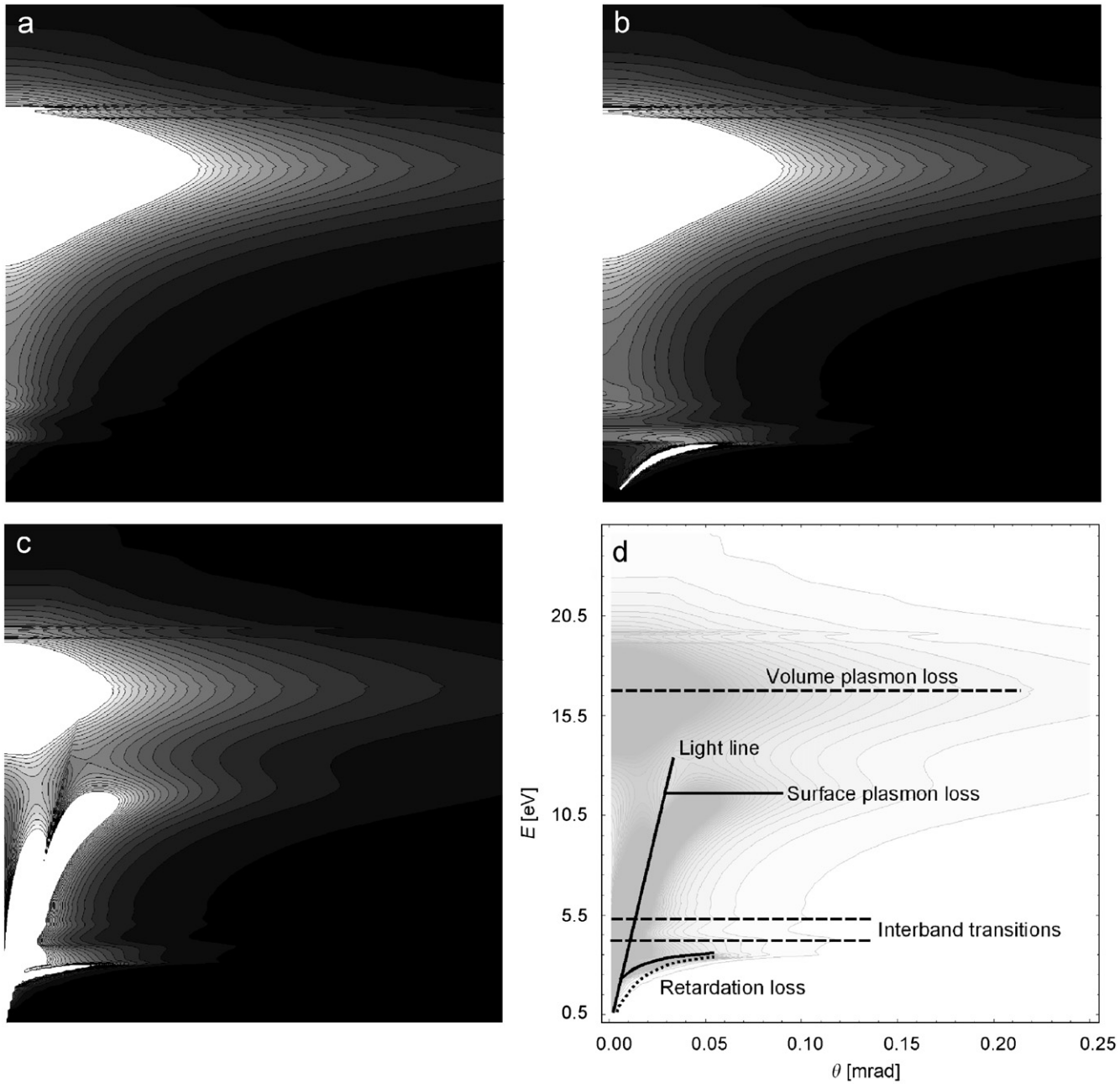

Fig. 1. Calculated scattering probabilities in the (E, θ)-plane of 300 keV electrons transmitting a Si film of 50 nm thickness. Plot (a) shows the volume contribution according to Eq. (1), (b) shows the volume contribution including retardation effects (Eq. (3)), and (c) shows volume, surface and retardation contributions according to Eq. (4). The plot in (d) schematically identifies the individual absorption features.

used are based on optical spectroscopy [26], the indirect band-gap signal (~1.1 eV) is not contained in the plots of Fig. 1. The solid line given by $E = c_L\,\theta$ (with $c_L = m_e v\,c$) runs along the main dispersion direction of the surface excitation, the individual branches along this light line are determined by the dispersion relations $\left|L^{+}(\theta,E)\right| = \text{Min.}$ and $\left|L^{-}(\theta,E)\right| = \text{Min.}$ The actual surface plasmon loss as observed in the calculated VEEL spectra can be found around 11 eV.

Fig. 2 shows the scattering probability P according to Eq. (4) for 200 keV electrons interacting with Si foils of 10 nm (a), 50 nm (b), 100 nm (c) and 1000 nm (d) thickness. Comparing Fig. 1(c) (50 nm Si, 300 keV) with Fig. 2(b) (50 nm Si, 200 keV) shows that a change of the electron energy from 300 to 200 keV mainly affects the scattering angle of the individual absorption features; due to the change of v, the slope of the light line $E = c_L\,\theta$ changes. In Fig. 3 the scattering probability of 200 keV electrons interacting with Si is shown for a fixed energy loss of 3 eV as a function of the scattering angle θ; curve (a) corresponds to $P_{vol,nr}$ according to Eq. (1) calculated for 100 nm Si, curve (b) corresponds to P_{vol} according to

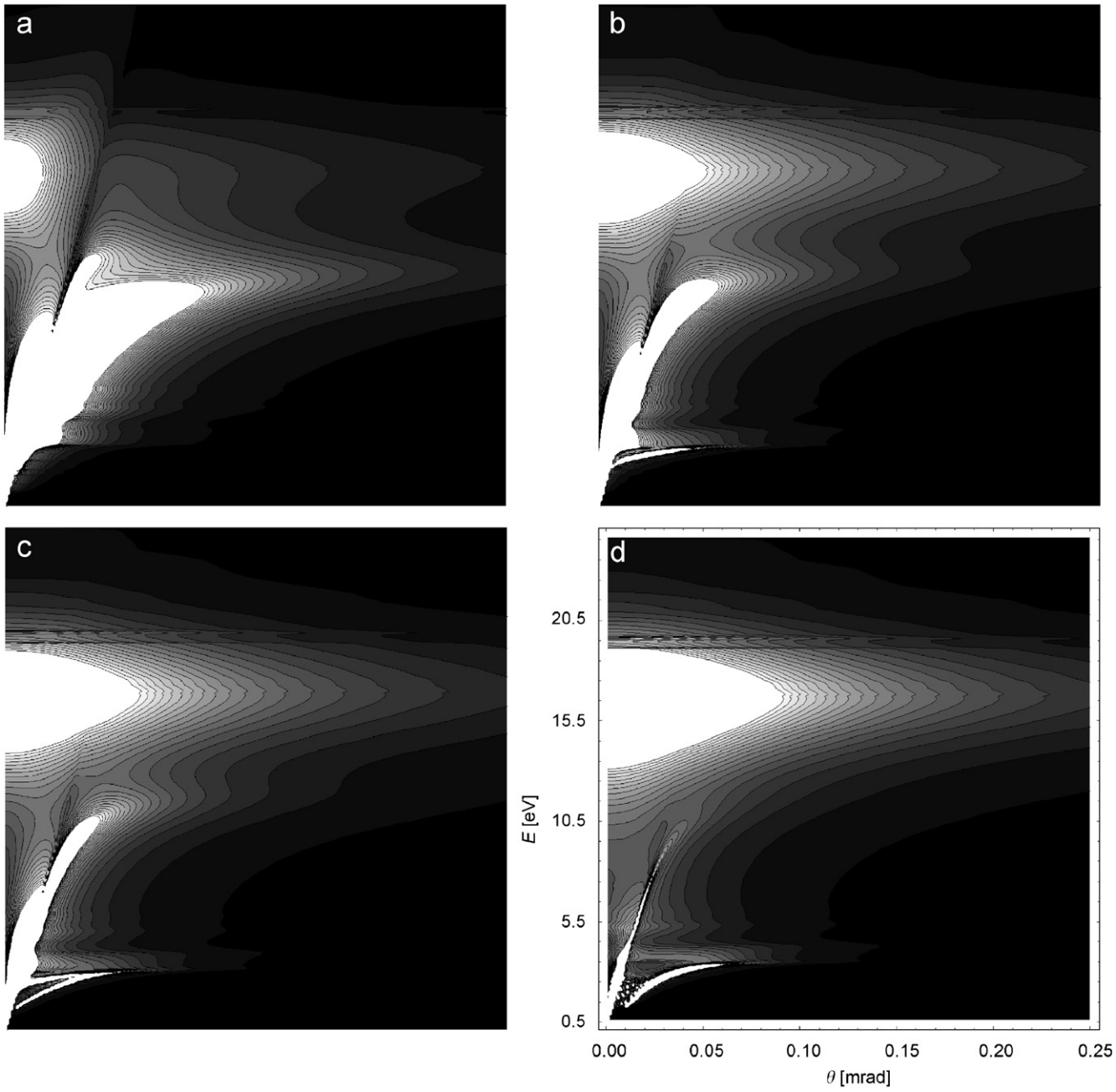

Fig. 2. Thickness dependency of the scattering probability. Calculated scattering probability in the (E, θ)-plane of 200 keV electrons transmitting a Si film of (a) 10 nm, (b) 50 nm, (c) 100 nm and (d) 1000 nm thickness. The scattering probability was calculated according to Eq. (4).

Eq. (3) calculated for 100 nm Si and, the other curves show P according to Eq. (4) calculated for the foil thickness indicated in each case.

Fig. 4 shows calculated and experimental VEEL spectra of Si. The thickness series of VEEL spectra in Fig. 4(a) was calculated according to Eq. (4). The collection angle used in the calculations was 2.1 mrad. Fig. 4(b) shows a thickness series of experimental VEEL spectra of Si recorded at 300 kV, the thickness is given in units of the inelastic mean free path λ_{in}. Considering an effective collection angle for a physical collection angle of 3.8 mrad and a probe semi-convergence angle of 19 mrad, the inelastic mean free path λ_{in} is ~130 nm.

4.2. Si_3N_4

Fig. 5 shows calculated scattering probabilities in the (E, θ)-plane of 200 keV electrons transmitting a 50 nm thick foil of Si_3N_4, analogous to Fig. 1. The scattering probability $P_{vol,nr}$ of the non-retarded volume contribution according to Eq. (1) is depicted in Fig. 5(a). Fig. 5(b) shows the volume-scattering probability P_{vol} according to Eq. (3),

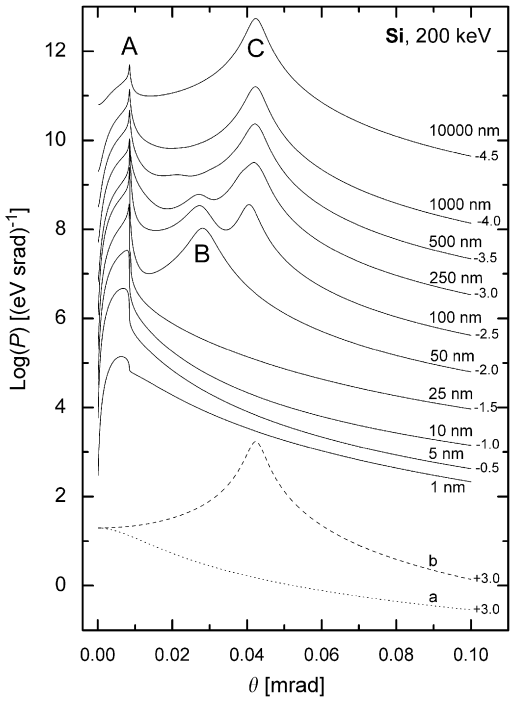

Fig. 3. Calculated scattering probabilities for a fixed energy loss E of 3 eV as a function of the scattering angle θ for 200 keV electrons transmitting a Si film. Curve (a) shows the volume contribution of a 100 nm thick film according to Eq. (1). Curve (b) shows the volume contribution of a 100 nm thick film according to Eq. (3). The other curves were calculated according to Eq. (4). The foil thickness is indicated in each case. The numbers running from +3.0 to −4.5 indicate the shifts on the y-axis.

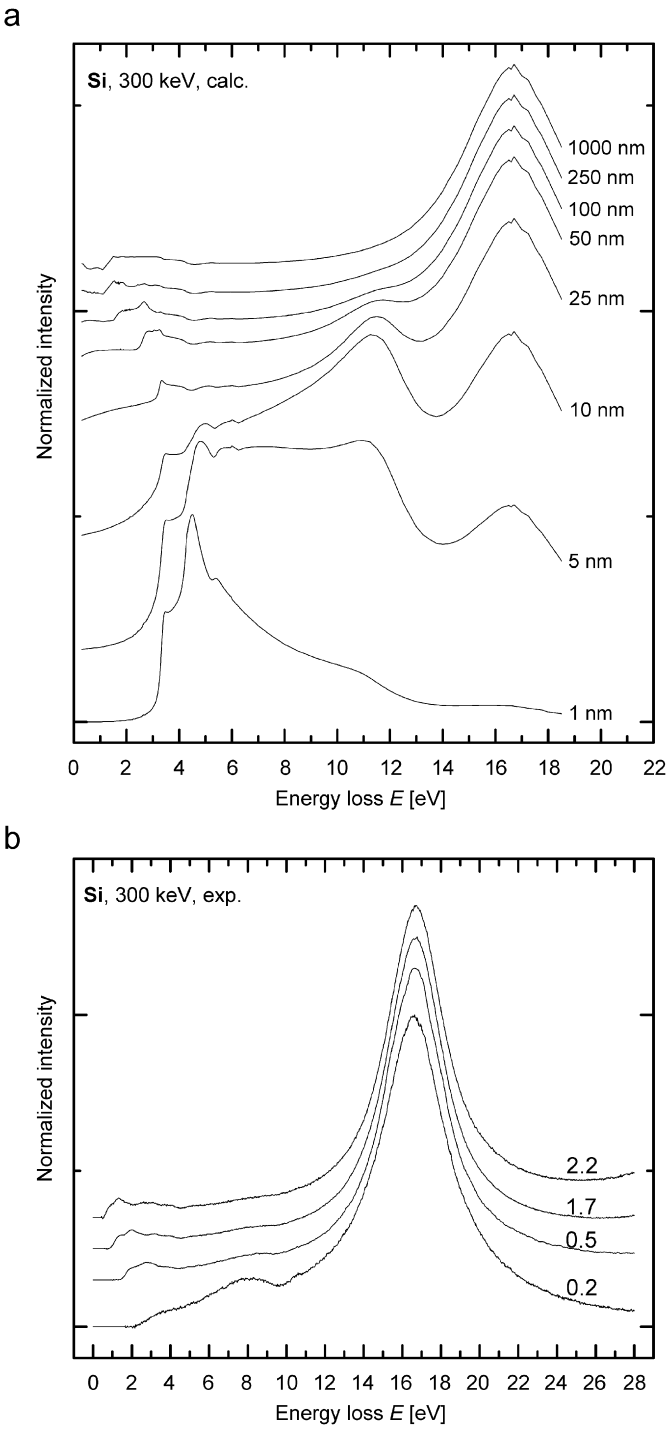

Fig. 4. VEEL spectra of Si (300 keV). (a) Series of spectra calculated according to Eq. (4) for the foil thickness indicated in each case. (b) Series of experimental spectra of Si recorded at 300 kV using a probe semi-convergence angle of 19 mrad and a collection angle of 3.8 mrad. The foil thickness is given in units of the inelastic mean free path λ_{in}; 0.2, 0.5, 1.7, 2.2. All spectra are normalized and for clarity shifted along the y-axis.

and the scattering probability P according to Eq. (4) is plotted in Fig. 5(c). The schematics in Fig. 5(d) identifies the main absorption features; the broad peak around 22.8 eV is caused by the excitation of the volume plasmon, the retardation peak can be found around 6.5 eV, where the real part of the dielectric function peaks. The surface excitation runs along the light line indicated in Fig. 5(d).

Fig. 6(a) shows a thickness series of calculated VEEL spectra of Si_3N_4. The spectra in Fig. 6(a) are based on Eq. (4) calculated for the thickness indicated in each case. In Fig. 6(b), an experimental spectrum of an amorphous Si_3N_4 film with a nominal thickness of about 25 nm is compared with a spectrum that was calculated according to Eq. (1). Since surface and retardation effects are not taken into account in the calculated spectrum of Fig. 6(b), the smooth intensity onset of this spectrum can unambiguously be identified as the band-gap signal.

4.3. GaAs

Fig. 7(a) shows a thickness series of calculated VEEL spectra of GaAs. Owing to the limited availability of dielectric data of GaAs, the spectra only cover an energy-loss range from ~0.5 to 6 eV. The volume plasmon and surface plasmon peaks, to be expected at ~16 and ~11 eV energy loss, are not contained in the spectra. In Fig. 7(b), a calculated spectrum of a 50 nm thick foil is compared with an experimental spectrum of a GaAs foil recorded in ⟨1 1 0⟩ zone-axis orientation. The main absorption features of the calculated spectrum match with the

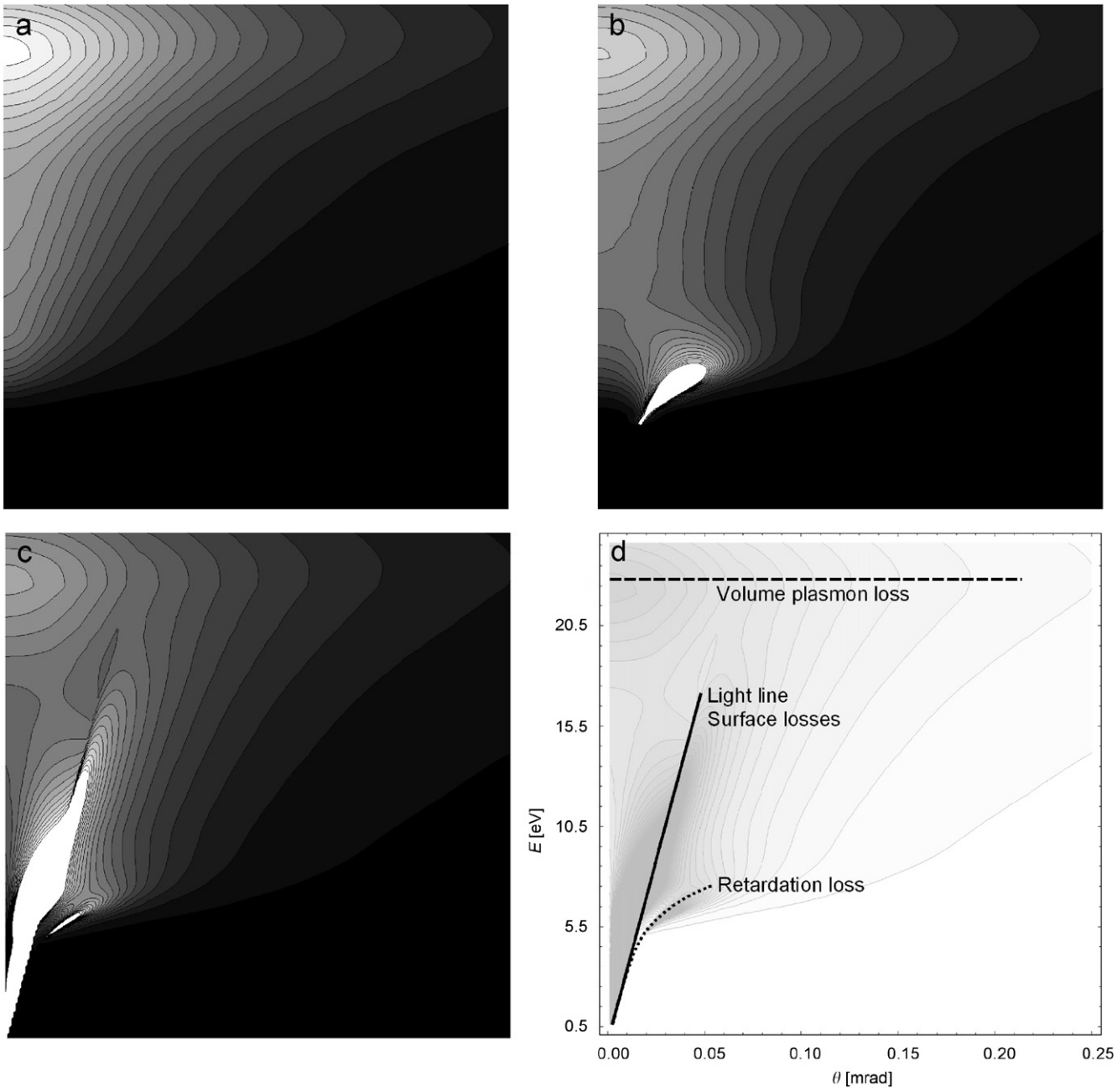

Fig. 5. Calculated scattering probabilities in the (E, θ)-plane of 200 keV electrons transmitting a Si_3N_4 film of 50 nm thickness. (a) Shows the volume contribution according to Eq. (1), (b) shows the volume contribution according to Eq. (3), and (c) shows the scattering probability according to Eq. (4). The plot in (d) schematically identifies the individual contributions.

experimental one. Owing to the limited energy resolution (~200 meV) and the noise present in the experimental spectrum, the detailed fine structure of the calculated spectrum cannot be compared with the experimental spectrum. The inset in Fig. 7(b) shows the entire experimental GaAs spectrum. A specimen thickness of 0.51 in units of the inelastic mean free path λ_{in} can be deduced. Considering an effective collection angle for a physical collection angle of 2.1 mrad and a probe semi-convergence angle of ~20 mrad, the inelastic mean free path λ_{in} is ~87 nm. All calculated spectra in Fig. 7 are based on Eq. (4).

4.4. GaN

Fig. 8(a) shows calculated VEEL spectra of GaN. Spectrum (a) was calculated according to Eq. (1) and spectrum (b) was calculated according to Eq. (3). All other spectra in Fig. 8(a) were calculated according to Eq. (4). Fig. 8(b) compares an experimental spectrum of GaN with a spectrum calculated for a foil thickness of 50 nm according to Eq. (4). The experimental spectrum in Fig. 8(b) is taken from a GaN film with a thickness of 0.42 in units of the inelastic mean free path λ_{in}.

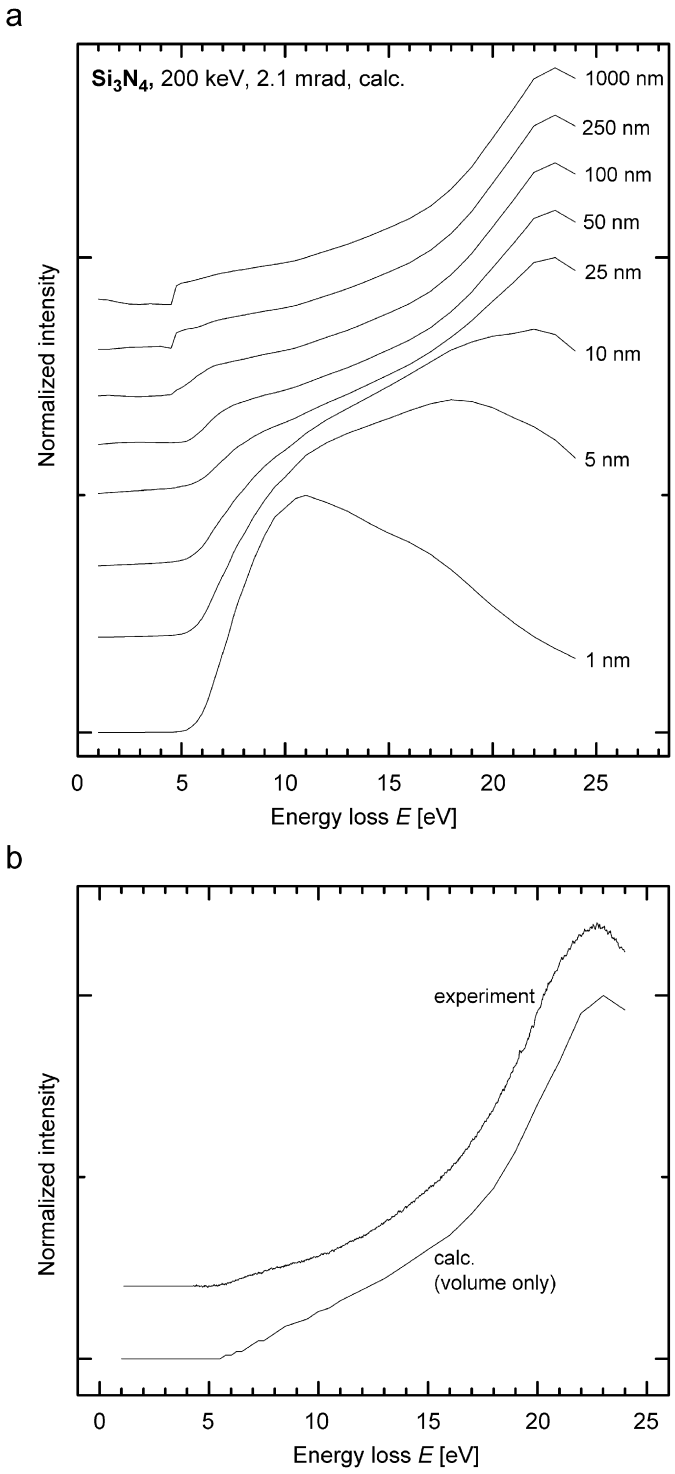

Fig. 6. VEEL spectra of Si_3N_4 (200 keV). (a) Series of spectra calculated according to Eq. (4) for the foil thickness indicated in each case. (b) An experimental spectrum of an amorphous Si_3N_4 film with a nominal thickness of 25 nm is compared with a spectrum that is calculated according to Eq. (1). All spectra are normalized and for clarity shifted along the y-axis.

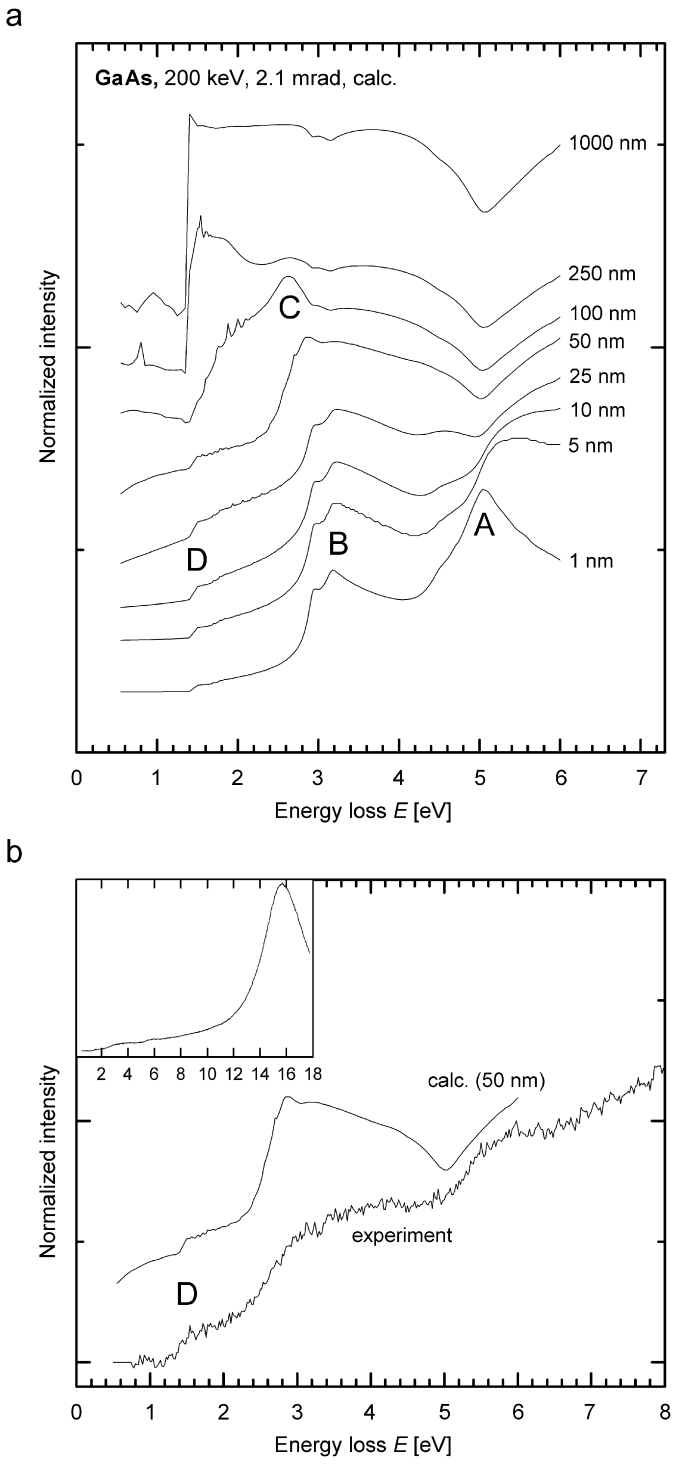

Fig. 7. VEEL spectra of GaAs (200 keV). (a) Series of spectra calculated according to Eq. (4) for the foil thickness indicated in each case. (b) An experimental spectrum of a GaAs film (0.51 λ_{in}) is compared with the spectrum calculated for a foil thickness of 50 nm. All spectra are normalized and for clarity shifted along the y-axis.

Considering an effective collection angle for a physical collection angle of 2.1 mrad and a probe semi-convergence angle of ~20 mrad, the inelastic mean free path λ_{in} is ~101 nm.

4.5. CdSe

Fig. 9 shows calculated VEEL spectra of wurtzite CdSe. Spectrum (a) was calculated according to Eq. (1) and

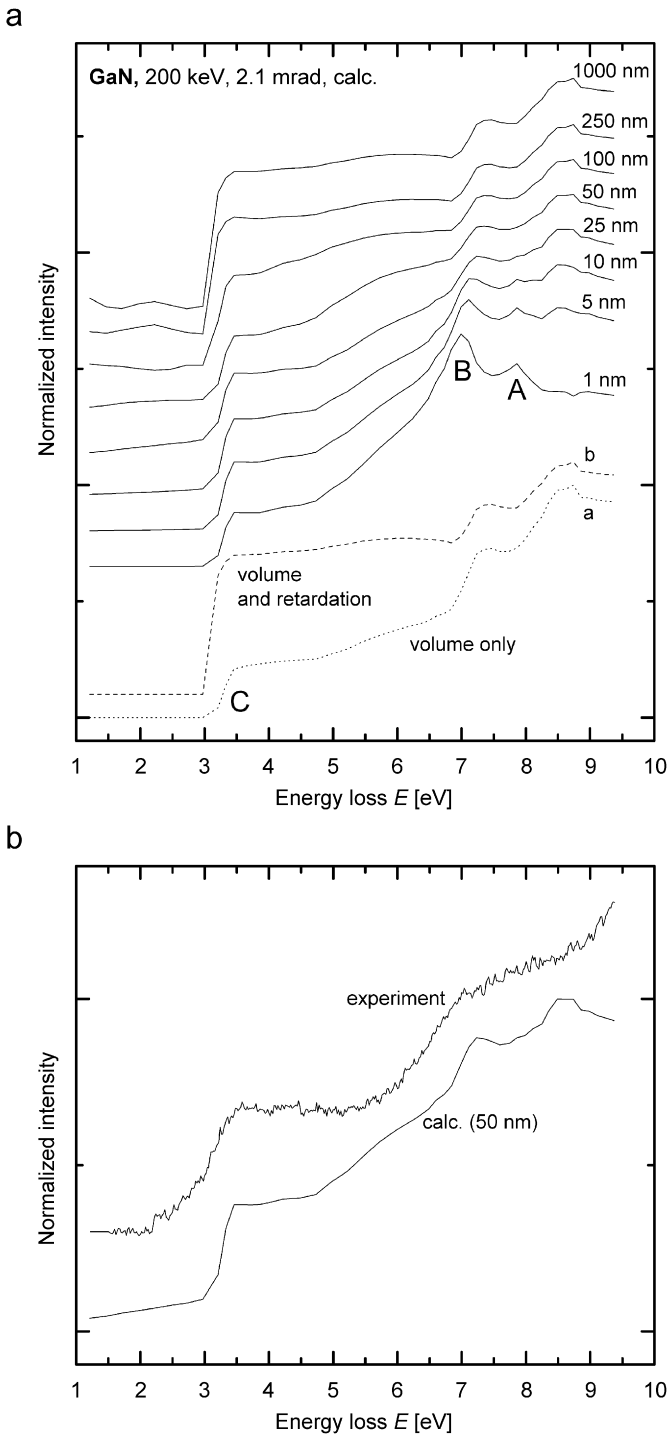

Fig. 8. VEEL spectra of GaN (200 keV). (a) Spectrum (a) is calculated according to Eq. (1) and spectrum (b) is calculated according to Eq. (3). The other spectra were calculated according to Eq. (4) for the foil thickness indicated in each case. (b) An experimental spectrum of a GaN film (0.42 λ_{in}) is compared with the spectrum calculated for a foil thickness of 50 nm. All spectra are normalized and for clarity shifted along the y-axis.

spectrum (b) was calculated according to Eq. (3). The other spectra in Fig. 9 were calculated according to Eq. (4) for the foil thickness indicated in each case.

5. Discussion

On the basis of the dielectric theory, the inelastic electron scattering of thin foils of Si, Si_3N_4, GaAs, GaN and CdSe was analyzed. For a series of different foil thicknesses, low-loss scattering probabilities and VEEL spectra were calculated under the assumption that the dielectric function is known. Provided that low-loss EEL spectra solely contain bulk contributions, including bulk retardation losses, the intensity of any absorption feature in a single-scattering VEEL spectrum should linearly increase with the thickness of the sample, see Eqs. (1) and (3). Any deviation from this behavior must be explainable by the finite size of the sample, particularly by surface effects. For all materials investigated, calculated single-scattering low-loss EEL spectra show a non-linear thickness dependency.

5.1. Si

The real part of the dielectric function of Si is sharply peaked at 3.3 eV with a value exceeding 43 [26]. The condition for the emission of Cerenkov radiation is thus fulfilled for electrons with an energy exceeding $eV_c \approx 5$ keV. Comparing Figs. 1(a) with 1(b), the impact of the retardation of the electron on the scattering distribution

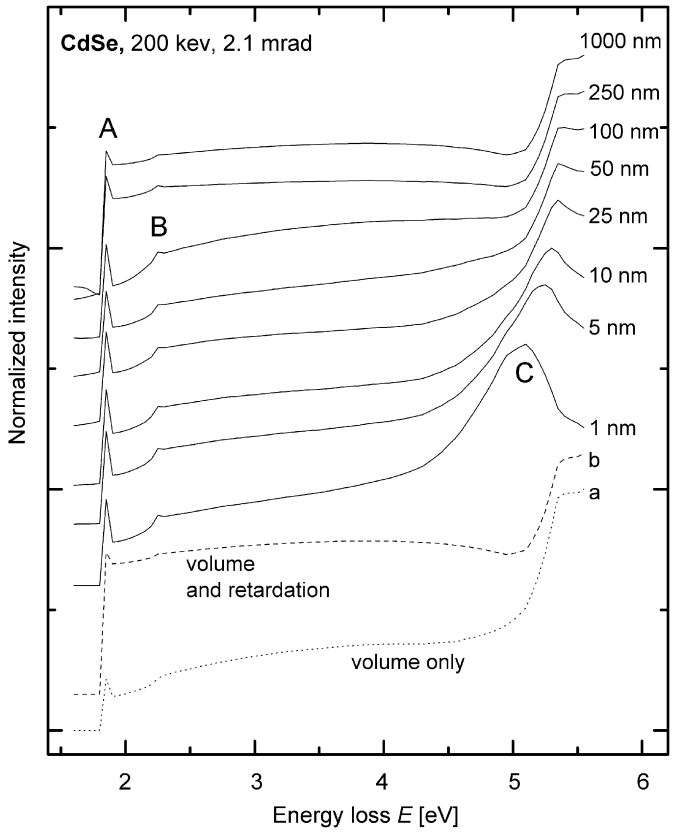

Fig. 9. Series of VEEL spectra of wurtzite CdSe (200 keV). Spectrum (a) is calculated according to Eq. (1) and spectrum (b) is calculated according to Eq. (3). The other spectra were calculated according to Eq. (4) for the foil thickness indicated in each case. All spectra are normalized and for clarity shifted along the y-axis.

in the (E, θ)-plane becomes apparent; the retardation leads to an arc-shaped intensity maximum between about 1 and 4 eV. For the non-retarded case the scattering probability is maximal at $\theta = 0$, whereas for the case retardation is taken into account, the maximum is shifted to finite values of θ, see also curves (a) and (b) in Fig. 3. Hence, the arc-shaped feature below 4 eV in Fig. 1(b) can be identified as a Cerenkov-loss peak.

Fig. 1(c) contains a similar absorption feature; an arc-shaped intensity maximum branched with the light line around 2 eV. The absorption feature in Fig. 1(c) is, however, different from the Cerenkov-loss peak in Fig. 1(b). The feature in Fig. 1(c) can be associated with the excitation of a guided light mode that is determined by the dispersion condition $|L^+| = \text{Min}$. The actual bulk Cerenkov-loss signature cannot be seen in Fig. 1(c). This means that if surface effects are taken into account (Fig. 1(c)), the volume retardation loss becomes negligible for a Si foil of 50 nm. The thickness series of $E-\theta$ plots in Fig. 2 shows that the arc-shaped absorption features in Figs. 1(b) and 1(c) have indeed different origins; for a foil thickness of 50 nm the absorption feature related to the excitation of guided light modes is dominant (see Fig. 2(b)), at a thickness of 100 nm both features—guided light mode and Cerenkov-loss feature—are equally present (Fig. 2(c)), whereas at 1000 nm the Cerenkov-loss peak has solely remained (Fig. 2(d)). The thickness series of calculated scattering probabilities for an energy loss of 3 eV in Fig. 3 illustrates in more detail the thickness dependency of these two absorption features. Apart from a surface mode observable below 0.01 mrad, labeled A, two maxima, B and C, can be identified. The relative intensity of absorption feature B decreases with increasing foil thickness. Furthermore, it moves to lower θ values. The position of feature C remains unchanged. The relative intensity of peak C increases with increasing foil thickness. Peak B can be associated with the guided light mode discussed above, whereas the invariant feature C corresponds to the Cerenkov-loss peak. This peak is not visible for foil thicknesses below ~100 nm. The invariant bulk retardation peak C is also reproduced in curve (b) of Fig. 3 where the scattering probability without considering surface effects P_{vol} is plotted.

Fig. 4 illustrates how the Cerenkov losses and the energy losses that are due to the excitation of the guided light modes impact VEEL spectra. For foil thicknesses exceeding ~25 nm, the spectra in Fig. 4(a) reveal a broad absorption feature between 1.5 and 4.5 eV. Except for the Si spectrum of 0.2 λ_{in} thickness, this spectral signature is also observable in the experimental spectra shown in Fig. 4(b). For very thin foils, there seems to be a mismatch between calculated and experimental spectra of Si. This mismatch is likely caused by the oxidized surface of the Si sample used for the measurements. The calculated as well as the experimental series of spectra in Fig. 4, give the impression that the low-loss retardation absorption feature below ~5 eV moves towards lower energy losses with increasing foil thickness. This behavior was shown by a thickness series of experimental VEEL spectra of Si by Stöger-Pollach et al. [29]. However, from the discussion above it is clear that it is not the Cerenkov-loss peak that moves towards lower energies. For foil thicknesses smaller than 250 nm, the absorption feature below 5 eV is dominated by energy losses that are due to the excitation of the guided light mode. Only for foil thicknesses above 250 nm, the Cerenkov-loss peak becomes dominant. The low-loss absorption feature remains then stationary. The seeming move of the Cerenkov-loss peak from higher to lower energies between 50 and 250 nm foil thickness [29], is in fact a transition between two different retardation absorption features; the guided light mode and the actual Cerenkov-loss peak.

The series of spectra in Fig. 4(a) reveals that for Si foils thinner than 25 nm, surface effects dominate the low-loss scattering. These surface effects cause an apparent, thickness-dependent modulation of some of the spectral signatures. Although these modulations cannot be observed at foil thicknesses exceeding 25 nm, a small contribution that is due to the excitation of the surface plasmon at ~11 eV energy loss can still be found at a foil thickness of 50 nm.

It can be summarized that in the case of Si, retardation effects (guided light mode and Cerenkov losses) significantly alter the low-loss electron scattering for foil thicknesses between 25 and 1000 nm. For foils thinner than 25 nm, surface contributions dominate the VEELS signal.

5.2. Si_3N_4

Silicon nitride has a direct band-gap with a transition energy of about 5 eV [30]. The real part of the dielectric function of Si_3N_4 is peaked at 6.5 eV with a maximum value of 7.3. The condition for the emission of Cerenkov radiation is thus fulfilled for electrons exceeding $eV_c \approx$ 40 keV. However, since the dielectric function of Si_3N_4 runs smoother than the one of Si, a different behavior is expected. Comparing Fig. 1 with Fig. 5 reveals that these two materials indeed show clearly different scattering behaviors. Due to the different characteristics of the dielectric function, particularly because of the lower maximum value of ε_1 compared to Si, the appearance of distinctive energy losses related to retardation effects is suppressed, see Fig. 5. Comparing the experimental spectrum shown in Fig. 6(b) with the spectrum calculated according to Eq. (1), reveals that for Si_3N_4 bulk retardation effects and finite-sample effects hardly alter the main spectral characteristic.

However, retardation and surface effects are also present in the case of Si_3N_4. The series of spectra in Fig. 6(a) shows that for foils thinner than ~25 nm, surface contributions are dominant. Furthermore, for foils exceeding ~100 nm in thickness, the onset of the intensity is altered by retardation effects. Owing to the increasing contribution of volume

retardation losses, the main intensity onset moves to lower energies with increasing foil thickness. For foil thicknesses exceeding ~250 nm, the onset becomes stationary, i.e., the bulk retardation loss is the dominant feature causing a sharp step at 4.5 eV. Hence, if the finite size of the foil and retardation effects are taken into account, the intensity onset does not properly reproduce the band-gap signal for foils exceeding ~100 nm in thickness. Analyzing the intensity onset in terms of measuring the band-gap energy, would result in a thickness-dependent gap energy. Yet, below about 4 eV energy loss, no extra intensity maxima or distinct intensity modulations due to potential surface or retardation effects can be observed.

It can be summarized that in the case of Si_3N_4, retardation, surface and finite sample effects are less pronounced than in the case of Si. However, for foils thinner than 25 nm, surface contributions dominate the low-loss scattering. And for foils exceeding ~100 nm in thickness, the increasing contribution of the bulk retardation loss leads to a thickness-dependent intensity onset. Hence, for this thickness regime, the intensity onset cannot be identified with the band-gap signal.

5.3. GaAs

The dielectric functions of Si and GaAs look qualitatively and quantitatively very similar. The real part of the dielectric function of GaAs is sharply peaked at 2.85 eV with a maximum value of 24.2 and it becomes negative at 4.7 eV. As mentioned above, the real part of the dielectric function of Si peaks at 3.3 eV with a value above 40 and it becomes negative at 4.2 eV. The condition for the emission of Cerenkov radiation is in Si fulfilled for electrons with an energy exceeding $eV_c \approx 5$ keV. For GaAs, the critical electron energy is about 10 keV. Although the absolute values of the maxima and minima have lower values in GaAs than in Si, the fact that both functions behave similarly leads to the expectation that their low-loss electron scattering should be similar as well. The main qualitative difference between GaAs and Si is that the band gap of GaAs at 1.4 eV is direct, whereas the band gap of Si at 1.1 eV is indirect.

Plots of the scattering probability in the (E, θ)-plane of GaAs (not shown) confirm this expectation. For the case that surface contributions are not taken into account, the dominant absorption feature is the volume retardation peak. However, if the finite size of the sample is taken into account the low-loss scattering between 1.5 and 3.5 eV of foils thinner than ~100 nm is dominated by losses due to the excitation of a guided light mode. Analogous to Si, there is a transition between guided light mode and bulk retardation peak. In case of GaAs, this transition is more complex than in Si. However, similar to Si, the transition between guided light mode and Cerenkov-loss peak causes a seeming shift of the main low-loss feature. This seeming shift is documented in the thickness series of VEEL spectra in Fig. 7(a). The thickness series of spectra reveals that for foils thinner than ~25 nm, peak A moves to higher energy losses with increasing sample thickness. For foils exceeding 25 nm in thickness, peak A becomes stationary. Apart from this surface effect, the transition between guided light mode and volume retardation peak leads to a thickness-dependent absorption feature that is located between 1.5 and 3.5 eV energy loss, similar to the case of Si. There is a transition from peak B to C. However, for foils thinner than ~250 nm, the band-gap-induced intensity onset at ~1.4 eV, labeled with D, is hardly affected by these retardation effects, namely by the guided light modes and by the Cerenkov-loss peak. However, the slope in front of the intensity onset D changes with the thickness of the sample. In Fig. 7(b), an experimental spectrum of GaAs recorded at 200 kV is compared with a spectrum calculated for a thickness of 50 nm according to Eq. (4). Although retardation effects alter the spectral region in front of the band gap, the band gap of ~1.4 eV (peak C) can clearly be identified.

In summary, if the foil thickness is below ~25 nm, surface effects alter the bulk contribution of GaAs. Finite-sample effects (guided light mode) and bulk retardation effects significantly impact the low-loss electron scattering of GaAs for foil thicknesses between 25 and 1000 nm. Although these retardation effects impact VEEL spectra of GaAs at energy loss that are above the band-gap energy, the band-gap signal can clearly be identified. It is therefore possible to extract the correct band-gap energy of GaAs from VEEL spectra provided that the thickness of the foil is below ~250 nm.

5.4. GaN

The real part of the dielectric function of GaN is peaked at 3.3 eV with a value of 7.3. Hence, similar to Si_3N_4, $eV_c \approx 40$ keV. For 200 keV electrons, the condition for the emission of Cerenkov radiation is fulfilled for energy losses smaller than 6.8 eV. The band-gap energy of GaN has been measured by VEELS independently by several groups using different data analysis methods [4,7,8,31,32]. The known band-gap energy of GaN has been identified in all of these cases. The intensity onset C in spectrum (a) of Fig. 8(a), which contains non-retarded volume contributions only, reflects the band-gap signal of GaN. This kind of behavior is presumed if the band-gap energy is measured by analyzing experimental VEELS data on the basis of Eq. (1). Including bulk retardation, see curve (b) in Fig. 8(a), the intensity onset is shifted towards lower energies. However, if apart from the bulk retardation surface contributions are taken into account as well, see the spectra in Fig. 8(a), the impact of the volume retardation on the band-gap signal becomes negligible for foil thicknesses smaller than 100 nm. The spectra 1–50 nm reveal the proper band-gap signal, comparable to the "volume-only" case shown in curve (a). Only for foil thicknesses exceeding 100 nm, bulk retardation starts to interfere with the band-gap signal. Hence, it can be stated

that provided that the thickness of the foil is below ~100 nm, retardation effects do not alter the band-gap signal as observed in VEEL spectra of GaN.

However, retardation effects not only alter the intensity onset C for foils exceeding 100 nm in thickness, they also impact the spectral area between the peaks C and B. With increasing foil thickness the intensity between 3.5 and 7 eV increases, clearly deviating from the "volume-only" case shown in curve (a). The spectra calculated for 25 and 50 nm foil thickness show the closest similarity to the "volume-only" spectrum (a).

Apart from the retardation effects, surface effects modulate VEEL spectra of GaN for foils thinner than ~25 nm; peak A disappears and peak B moves to higher energy losses with increasing foil thickness. For foils exceeding ~25 nm in thickness, peak A and B represent the bulk absorption feature as observable in the "volume-only" spectrum of curve (a).

It can be concluded that a correct value for the band-gap energy of GaN can be extracted from low-loss EEL spectra, provided that the sample thickness does not exceed 100 nm. This finding is in agreement with various experimental results based on the analysis of VEEL spectra [4,7,8,31,32]. However, only for foil thicknesses between 25 and 50 nm, a Kramers-Kronig analysis on the basis of Eq. (1) of a VEEL spectrum would give a reasonable measure for the dielectric function. For foils thinner than ~25 nm, surface effects result in a thickness dependent modulation of the bulk absorption feature.

5.5. CdSe

The real part of the dielectric function of CdSe in [0 0 0 1] direction is maximal at 1.85 eV with a value of ~10 (at 15 K). This very distinct maximum is associated with an exciton that results in peak A of the calculated VEEL spectra in Fig. 9 [28]. Similar to peak A, peak B at 2.25 eV is also caused by an exciton [28]. Although the relative intensities of the excitonic peaks A and B depend on the foil thickness, their positions do not depend on the foil thickness. The intensity onset, dominated in all spectra of Fig. 9 by peak A, is invariant. In contrast to the excitonic peaks A and B, peak C, which is due to interband transitions [28], moves to higher energies with increasing foil thickness, approaching the bulk position at a foil thickness of ~25 nm.

Comparing spectrum (a) in Fig. 9 with spectrum (b), the impact of the retardation becomes apparent. Retardation leads to an increase of the spectral intensity between 2 and ~5 eV energy loss. Although the positions of peaks A and B are invariant, the intensity between the peaks A, B and C increases with increasing foil thickness above 100 nm. Apart from this retardation contribution and the shift of peak C with increasing foil thickness for foils thinner than 25 nm, no surface, finite sample or retardation effects are observable.

From all the materials investigated, the VEEL spectra of CdSe show the least thickness dependency. The presence of an excitonic peak likely explains the invariant intensity onset. However, Fig. 9 reveals that bulk retardation contributions lead to an increase of the scattering intensity between ~2 and 5 eV for foils exceeding 100 nm in thickness. For foils thinner than 25 nm, surface effects alter the position of a bulk absorption feature.

5.6. Trends

The results presented in Section 4 and discussed above indicate that the materials investigated can be split into two groups. Although all five materials potentially show bulk retardation effects, the impact of retardation effects, namely energy losses due to the excitation of guided light modes and Cerenkov radiation, is clearly different for Si and GaAs on the one hand and Si_3N_4, GaN and CdSe on the other hand.

For all foil thicknesses investigated, VEEL spectra of Si and GaAs contain distinct absorption features that are caused by retardation effects. For foil thicknesses below ~100 nm, the retardation absorption feature is dominated by energy losses due to the excitation of guided light modes. And for foil thicknesses exceeding ~250 nm in thickness, the retardation absorption feature is dominated by Cerenkov losses. The transition from the guided light mode to the Cerenkov loss leads to a seeming shift of the dominant low-loss absorption feature. In addition to these retardation absorption features, surface effects are observable. For samples thinner than 25 nm, VEEL spectra of Si and GaAs are impacted by surface effects. These surface effects result in thickness dependent shifts of the actual bulk absorption feature above the band-gap signal. The origin of these shifts is not clear. Since for all thicknesses the same dielectric function was used, it can be ruled out that the shifts are related to electronic states that emerge due to confinement. It seems likely that the shifts emerge from superposing the bulk absorption features on specific surface modulations of the VEEL spectra. With increasing thickness the impact of surface modulation on the bulk absorption feature decreases, explaining the thickness-dependent shifts.

Owing to surface and retardation effects, analyzing VEEL spectra of Si and GaAs on the basis of Eq. (1) would result in misleading dielectric data. There is no thickness regime where both types of effects, surface and retardation, can be neglected.

For the other materials investigated, Si_3N_4, GaN and CdSe, where the dielectric function runs smoother, the impact of surface and retardation losses is less pronounced. No extra intensity maxima due to retardation effects are observable. However, for foils exceeding 100 nm in thickness, bulk retardation effects lead to a gradual increase of the low-loss spectral intensity with increasing foil thickness. For foils thinner than 25 nm, surface effects lead to thickness dependent modulation of the dielectric bulk absorption features. For foils with a thickness between 25 and 100 nm, surface and retardation effects

are very small and do not significantly alter the dielectric bulk absorption features. For this thickness regime, correct band-gap energies can be extracted from VEEL spectra and a Kramers-Kronig analysis of the low-loss spectrum could result in correct transition energies and qualitatively correct band-structure models. It must, however, be mentioned that even for foils between 25 and 100 nm, additional intensity in front of the known band-gap signal can be observed (see Figs. 6 and 8). Since the imaginary part of the dielectric function in front of the band gap is zero, this smooth, spurious contribution must be related to retardation effects. Although this additional intensity is hardly modulated, it certainly complicates the background removal of the zero-loss peak contribution.

Comparing the first group of materials (Si and GaAs), with the second group (Si_3N_4, GaN, and CdSe), shows that the impact of retardation effects (Cerenkov losses and guided light modes) on VEELS depends on the characteristics of the dielectric function of the material. It is, in particular, the maximum of the real part of the dielectric function that is crucial. Although for all materials investigated the bulk condition for the emission of Cerenkov radiation is fulfilled, the observable retardation effects differ a lot. Retardation effects are maximal where the real part of the dielectric function is maximal. Peaks due to the excitation of guided light modes or Cerenkov losses roughly coincide with maxima of the dielectric function (Si and GaAs). If these maxima are less pronounced, no additional absorption peaks are observable (Si_3N_4, GaN, and CdSe). In the cases of Si and GaAs, retardation peaks impact VEEL spectra for all foil thicknesses investigated. In the cases of Si_3N_4, GaN, and CdSe, distinct retardation effects can only be observed for foil thicknesses exceeding 100 nm.

Surface effects depend less on the characteristic of the dielectric function. For all materials investigated, surface effects can lead to thickness dependent modulations of bulk absorption features. For foils thinner than 25 nm, all five materials investigated show thickness dependent modulation of bulk dielectric absorption features.

It is suggested that the impact of retardation effects on VEEL spectra of thin foils can be estimated by analyzing the probability of the emission of Cerenkov radiation of the corresponding bulk materials. Even though the present study showed that thin foils of materials (<100 nm) hardly show bulk Cerenkov effects, the probability of the emission of Cerenkov radiation of the bulk material gives an estimation of the impact of retardation effects, including retardation effects related to the finite size of the sample, like guided light modes. The number of Cerenkov photons emitted by a unit charge per unit of path length in a bulk material is given by

$$P_{\text{Cerenkov}} = \frac{1}{c^2} - \frac{1}{v^2 \varepsilon_1}. \quad (6)$$

This number, P_{Cerenkov}, depends on the speed of the charged particle v (on the primary electron energy E_0) and on the real part of the dielectric function ε_1. If P_{Cerenkov} is normalized by $1/c^2$, a function P^* is obtained that describes the probability of the emission of bulk Cerenkov photons in respect to the maximal emission rate, i.e., $P^* = P^*(E_0, \varepsilon_1)$. The contour plot in Fig. 10 depicts this normalized emission rate P^* as a function of E_0 and ε_1. If P^* is smaller or equal zero, no bulk Cerenkov radiation is emitted and no retardation effects are expected. This corresponds to the condition mentioned in the introduction; only if $v > c/\sqrt{\varepsilon_1}$, Cerenkov losses become feasible. The solid bold line in Fig. 10 marks this condition; for pairs of E_0 and ε_1 that lie on the left and below this line, retardation does not occur. With increasing E_0 and ε_1, the emission probability P^* increases. On grounds of the above analysis, it is postulated that the impact of retardation effects, such as guided light modes or Cerenkov losses, on low-loss EEL spectra increases with increasing P^*. Hence, correlating experimental and theoretical data with values of P^*, makes it feasible to qualitatively forecast the impact of retardation losses on low-loss EEL spectra.

The maximum values of ε_1 of the materials investigated are 43.3 for Si, 24.2 for GaAs, 7.3 for Si_3N_4, 7.3 for GaN, and 10.0 for CdSe. For each pair of variates of E_0 and ε_1, a

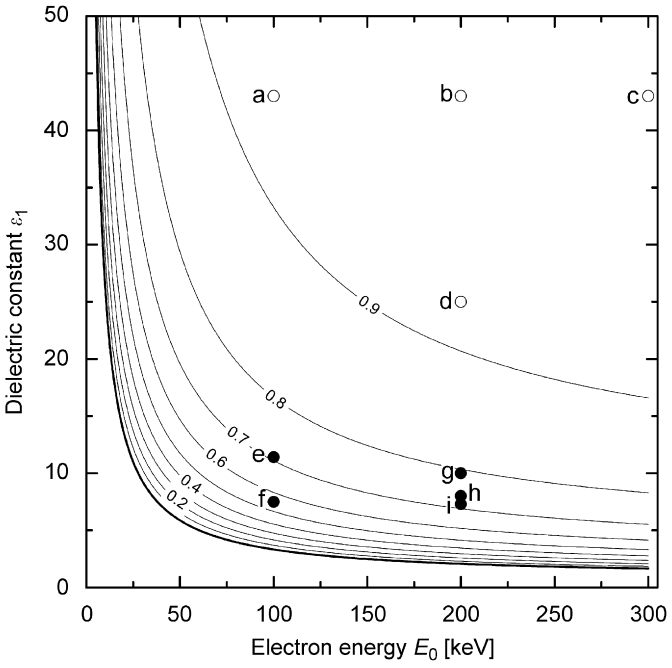

Fig. 10. Contour plot of $P^*(\varepsilon_1, E_0)$, for details see text. The bold solid line corresponds to the condition for the emission of Cerenkov radiation; for pairs of E_0 and ε_1 that are on the left or below this line, retardation effects are not possible. The open circles indicate measurements where strong retardation effects were observed, whereas the full circles indicate measurements where retardation effects were marginal. Points (a), (b) and (c) are based on results of Si from Refs. [29,33] and from the present work; point (d) is based on GaAs from Ref. [29] and the present work, point (e) is based on results of $SrTiO_3$ [6], point (f) is based on results of AlN [21], point (g) is based on CdSe from the present work, point (h) is based on InN [7], and point (i) is based on GaN and Si_3N_4 from the present work. The transition between strong and weak retardation effects is in the range of $P^* = 0.9$.

value of P^* can be found in the contour plot of Fig. 10, see points c, d, g, and i. Si (300 keV) and GaAs (200 keV) showed strong retardation effects for typical STEM/TEM foil thicknesses, the corresponding values of P^* exceed 0.9 (points c and d). For Si_3N_4, GaN and CdSe, P^* is between 0.7 and 0.8 (points g and i). Si_3N_4, GaN and CdSe revealed weak retardation effects for typical STEM/TEM foil thicknesses. Using the contour plot in Fig. 10 to qualitatively estimate the impact of retardation effects on VEEL spectra, it can be summarized that for measurements that fall into areas where P^* is between zero and ~0.8, negligible or very weak retardation effects are expected for foils thinner than 100 nm, whereas for measurements that fall into the area where P^* is above ~0.9, strong retardation effects are expected independent of the foil thickness (either guided light modes or Cerenkov losses). Yet for all values of P^* non-retarded surface effects could potentially alter the low-loss electron scattering. It is clear that these guidelines are based on a very limited number of data points. However, experimental data obtained at electron energies between 100 and 200 keV from various publications and different materials support this guideline [1,6,7,21,29,33].

The analysis of the thickness dependency of the VEELS signal of all materials investigated shows that for foils thinner than 25 nm, the position of peaks associated with interband transitions can move to higher energies with increasing sample thickness (see Figs. 7–9). This effect must be surface related. The position of these peaks becomes, however, stationary for foils exceeding 25 nm in thickness, approaching the position which is obtained if only volume contributions are considered in the calculation. Surface-plasmon peaks can, however, be present even in samples that exceed ~25 nm in thickness, see Fig. 4(a). Mkhoyan et al. [33] recently proposed a method to separate invariant surface contributions from dielectric bulk contributions in VEEL spectra.

Whether retardation and surface effects impact a VEEL spectrum or not, could be tested by analyzing the experimental VEEL spectrum by a Kramers-Kronig analysis (see, e.g., [21]). Such an analysis on the basis of Eq. (1) would yield a first-guess dielectric function of the material. In a second step, this dielectric function could be used to calculate the VEEL spectrum using, however, Eq. (4) instead of Eq. (1). If the calculated spectrum does not match the experimental one, it is clear that surface and/or retardation effects significantly contribute to the experimental spectrum.

The impact of surface and retardation losses on VEEL spectra could be reduced if an experimental setup could be found that allows for blocking low-loss scattering at very small scattering angles. Although the scattering angles increase with decreasing primary electron energy, Figs. 1–3 and 5 reveal that the low-loss scattering due to surface excitations, bulk retardation and guided light modes is typically below 0.1 mrad (at 200 or 300 kV). Blocking the low-angle inelastic scattering would allow for recording VEEL spectra that are not affected by retardation and/or surface losses. The scattering intensity on the detector would strongly be reduced though. Furthermore, the realization of such a geometrical setup is complicated by the fact that typical semi-convergence angles of electron probes used in STEM are in the range of 10 mrad or larger.

6. Conclusions

On grounds of the analysis of the low-loss inelastic electron scattering of thin films of Si, Si_3N_4, GaN, GaAs and CdSe the following practical conclusions can be drawn:

- For foils thinner than 25 nm, surface effects can lead to shifts of bulk absorption features (see Figs. 7–9). Hence, using TEM foils thicker than 25 nm in VEELS, reduces the risk of having surface effects interfering with the actual bulk dielectric losses. However, even for samples exceeding 25 nm, the contribution of the surface plasmon peak can still be significant.
- The analysis of Si and GaAs showed that for experiments that have a P^* value exceeding 0.9, strong retardation effects are expected—independent of the actual foil thickness (see Fig. 10). For thin foils (<100 nm), losses due to the excitation of guided light modes dominate the retardation-loss peak. And for samples exceeding 250 nm, losses due to Cerenkov radiation dominate the retardation-loss peak. The retardation peaks can be found close to where the real part of the dielectric function peaks.
- The analysis of Si_3N_4, GaN and CdSe showed that for experiments that have a P^* value between 0.0 and 0.8, retardation effects are very small or negligible for foils thinner than 100 nm. For foils exceeding 100 nm in thickness, retardation effects can lead to a shift of the spectral intensity onset towards lower energies.

Considering both, surface and retardation effects, the most suitable specimen thickness for measuring bulk properties by VEELS of materials similar to the ones discussed in this article is above 25 nm, but below 100 nm, with $P^* < \sim 0.9$.

Acknowledgments

Part of the experimental work was performed at the National Center for Electron Microscopy, Lawrence Berkeley National Laboratory, supported by the Director, Office of Science, of the US Department of Energy (DoE) under Contract no. DE-AC03-76SF00098. The authors acknowledge the Ernst-Ruska Center, Forschungszentrum Jülich (Germany), for providing the S-Titan instrument that was used to record the experimental data shown in Fig. 4. This work is supported in part by the US Department of Energy (DoE) under Grant no. DE-FG02-03ER46057.

References

[1] P.E. Batson, K.L. Kavanagh, J.M. Woodall, J.W. Mayer, Phys. Rev. Lett. 57 (1986) 2729.
[2] J. Yuan, L.M. Brown, W.Y. Liang, J. Phys. C 21 (1988) 517.
[3] B. Rafferty, L.M. Brown, Phys. Rev. B 58 (1998) 10326.
[4] G. Brockt, H. Lakner, Micron 31 (2000) 435.
[5] R.H. French, H. Müllejans, D.J. Jones, G. Duscher, R.M. Cannon, M. Rühle, Acta Mater. 46 (1998) 2271.
[6] K. van Benthem, R.H. French, W. Sigle, C. Elsässer, M. Rühle, Ultramicroscopy 86 (2001) 303.
[7] J.R. Jinschek, R. Erni, N.F. Gardner, A.Y. Kim, C. Kisielowski, Solid State Commun. 137 (2006) 230.
[8] S. Lazar, G.A. Botton, M.-Y. Wu, F.D. Tichelaar, H.W. Zandbergen, Ultramicroscopy 96 (2003) 535.
[9] K. Kimoto, G. Kothleitner, W. Grogger, Y. Matsui, F. Hofer, Micron 36 (2005) 185.
[10] R. Erni, N.D. Browning, Ultramicroscopy 104 (2005) 176.
[11] D. Ugarte, C. Colliex, P. Trebbia, Phys. Rev. B 45 (1991) 4332.
[12] F.J. García de Abajo, A. Rivacoba, N. Zabala, N. Yamamoto, Phys. Rev. B 69 (2004) 155420.
[13] A. Howie, R.H. Milne, Ultramicroscopy 18 (1985) 427.
[14] H. Raether, Excitation of Plasmons and Interband Transistions by Electrons, Springer Tracts in Modern Physics, vol. 88, Springer, Berlin, 1980.
[15] E. Kröger, Z. Phys. 216 (1968) 115.
[16] C. von Festenberg, Z. Phys. 214 (1968) 464.
[17] C. von Festenberg, Z. Phys. 227 (1969) 453.
[18] R. Vincent, J. Silcox, Phys. Rev. Lett. 31 (1973) 1487.
[19] C.H. Chen, J. Silcox, Phys. Rev. Lett. 35 (1975) 390.
[20] R. Erni, N.D. Browning, Ultramicroscopy 107 (2007) 267.
[21] A.D. Dorneich, R.H. French, H. Müllejans, S. Loughin, M. Rühle, J. Microsc. 191 (1998) 286.
[22] E. Kröger, Z. Phys. 235 (1970) 403.
[23] R.H. Ritchie, Phys. Rev. 106 (1957) 874.
[24] R.F. Egerton, Electron Energy-Loss Spectroscopy in the Electron Microscope, second ed., Plenum Press, New York, 1996.
[25] S. Schamm, G. Zanchi, Ultramicroscopy 88 (2001) 211.
[26] E.D. Palik, Handbook of Optical Constants of Solids, 1985–1991.
[27] T. Kawashima, H. Yoshikawa, S. Adachi, S. Fuke, K. Ohtsuka, J. Appl. Phys. 82 (1997) 3528.
[28] S. Logothetidis, M. Cardona, P. Lautenschlager, M. Garriga, Phys. Rev. B. 34 (1986) 2458.
[29] M. Stöger-Pollach, H. Franco, P. Schattschneider, S. Lazar, B. Schaffer, W. Grogger, H.W. Zandbergen, Micron 37 (2006) 396.
[30] A. Iqbal, W.B. Jackson, C.C. Tsai, J.W. Allen, C.W. Bates, J. Appl. Phys. 61 (1987) 2947.
[31] A. Gutierrez-Sosa, U. Bangert, A.J. Harvey, C. Fall, R. Jones, Diam. Rel. Mater. 12 (2003) 1108.
[32] P. Specht, J.C. Ho, X. Xu, R. Armitage, E.R. Weber, R. Erni, C. Kisielowski, Solid State Commun. 135 (2005) 340.
[33] K.A. Mkhoyan, T. Babinec, S.E. Maccagnano, E.J. Kirkland, J. Silcox, Ultramicroscopy 107 (2007) 345.